JOURNAL OF SPACECRAFT AND ROCKETS
Vol. 34, No. 3, May–June 1997

Six-Degree-of-Freedom Entry Dispersion Analysis for the METEOR Recovery Module

Prasun N. Desai,* Robert D. Braun,* Richard W. Powell,† Walter C. Engelund,* and Paul V. Tartabini*
NASA Langley Research Center, Hampton, Virginia 23681-0001

A six-degree-of-freedom entry dispersion analysis for the multiple experiment transporter to Earth orbit and return mission is presented. This mission offers the capability of flying a recoverable science package in a microgravity environment. The recovery module has no active control system. Hence, uncertainties in the initial conditions prior to deorbit burn initiation, during deorbit burn and exoatmospheric coast phases, and during atmospheric flight affect the splashdown location. Thus, this investigation quantifies the impact of these various exoatmospheric and atmospheric uncertainties. Additionally, a Monte Carlo analysis is performed to statistically assess the splashdown dispersion footprint caused by multiple mission uncertainties. The Monte Carlo analysis showed that a 3-σ splashdown dispersion footprint with axes of 43.3 (long), −33.5 (short), and ± 10.0 n mi (crossrange) can be constructed. A 58% probability exists that the recovery module will overshoot the nominal splashdown site.

Nomenclature

α_T = total angle between the velocity vector and the vehicle's axis of symmetry, deg
β = sideslip angle, deg
γ = flight-path angle, deg
σ = angle of attack, deg

Introduction

Background

THE multiple experiment transporter to Earth orbit and return (METEOR) mission was launched aboard the inaugural flight of the Conestoga launch vehicle in October 1995. Formerly known as the commercial experiment transporter (COMET), the system consists of the Conestoga launch vehicle, a service module (SM), and a recovery module (RM). Unfortunately, due to a failure aboard the Conestoga during ascent, the launch vehicle and payload were lost.

Through the use of the RM, which re-enters approximately 20 days after launch, METEOR offered the capability of flying experiments to orbit in a microgravity environment and then the ability to recover them. The RM was originally designed by Space Industries, Incorporated, and an entry dispersion analysis of the mission was performed.[1–4] However, in 1995, EER Systems, Inc., took over the final development of the RM (Fig. 1) and modified the original mission (orbit altitude, spacecraft mass properties, and the nominal landing site). As a result, a six-degree-of-freedom (DOF) entry dispersion analysis of the new mission scenario was necessitated. Also, the reliability of previous dispersion analysis was questioned due to a lack of a complete aerodynamic database for the RM.[5] Thus, the present study was initiated to provide an independent assessment of the major program elements that could impact the vehicle splashdown location. Initial concerns focused on three issues: 1) development of a complete aerodynamic database from which to base the atmospheric flight simulations, 2) the magnitude of each of the mission uncertainties, and 3) the fidelity of the mission modeling.

Presented as Paper 96-0903 at the AIAA 34th Aerospace Sciences Meeting, Reno, NV, Jan. 15–18, 1996; received April 8, 1996; revision received Feb. 7, 1997; accepted for publication Feb. 7, 1997.

*Aerospace Engineer, Space Systems and Concepts Division. Member AIAA.
†Senior Research Engineer, Space Systems and Concepts Division. Member AIAA.

Mission Description

The mission scenario is as follows (Fig. 2). METEOR was to be launched into approximately a 250-n mi circular orbit from NASA Wallops Flight Facility having an orbital inclination of 40.5 deg. After approximately 20 days, the deorbit sequence begins. The attitude control system aboard the SM points the combined system to a specified attitude. With the use of a spin table, the RM is spun up to 73 rpm and separated from the SM. Because the RM has no active control system, the spin up provides stability to maintain its pointing attitude prior to and during the deorbit burn. Following a coast period (approximately one-half orbit), the deorbit burn is performed to initiate the entry of the RM. Shortly before the atmospheric passage (approximately 500 kft), the RM is despun to a nominal 6.5 rpm by a yo-yo despin device. This despin maneuver is performed to reduce the gyroscopic stability of the RM, thus allowing the vehicle's aerodynamic characteristics to reduce its angle of attack prior to peak heating. The vehicle aerodynamically decelerates from approximately 25,000 ft/s to subsonic speeds. At an altitude of 60 kft, a series of three parachute deployments begin to slow the RM before splashdown off the coast of Virginia. The RM is positively buoyant and would be picked up by a surface vessel so that the experiments can be recovered.

Analysis

Aerodynamics

The aerodynamic database utilized in the flight simulation studies was derived from a combination of computational fluid dynamics calculations and wind-tunnel and engineering code results. Because the flight traverses different flow regimes (rarefied, transitional, continuum), a range of solution methods were required to estimate the aerodynamics of the RM. Free molecular models were employed at altitudes above 394 kft (120 km), direct simulation Monte Carlo (DSMC) models[6] were used for altitudes between 295 kft (90 km) and 394 kft (120 km), and a Navier–Stokes solver[7] was applied at altitudes below 263 kft (80 km). The Navier–Stoke solutions were augmented with experimental data at Mach 6 and at Mach numbers between 1.60 and 2.85. Subsonic aerodynamic characteristics were obtained with a linearized potential flow solver.[8] In the transition region between 263–295 kft (80–90 km), the aerodynamics are obtained through linear interpolation. The aerodynamic characteristics of the METEOR RM are explained in greater detail in Refs. 5 and 9. Additionally, due to the RM's configuration similarity with the Mercury crewed entry capsule, dynamic stability aerodynamics were estimated based on Mercury capsule flight data.[10]

Six-DOF Trajectory Simulation

The trajectory analysis was performed using the six- and three-DOF versions of the Program to Optimize Simulated Trajectories

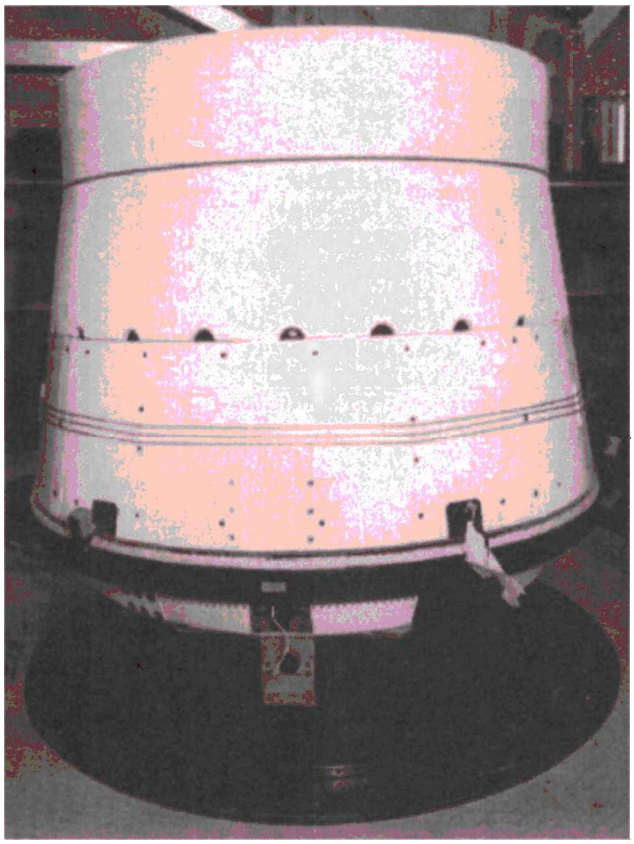

Fig. 1 Recovery module configuration.

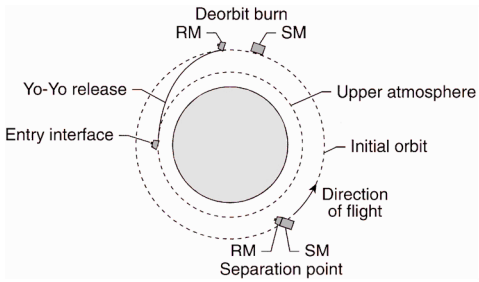

Deorbit sequence

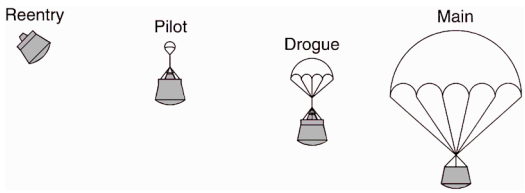

Parachute deployment sequence

Fig. 2 METEOR mission profile.

(POST).[11] This program has been utilized previously in similar applications.[12,13] The six-DOF version of this program was used to integrate the translational and rotational equations of motion from prior to the deorbit burn to parachute deployment. The three-DOF program was used to integrate the translational equations from parachute deployment to splashdown. The six-DOF simulation includes the Earth atmospheric (GRAM-95) (Ref. 14) and gravitational models, vehicle aerodynamics, mass properties and propulsion models, SM separation, and yo-yo release/despin models. The yo-yo release/despin is modeled using the method developed by Etter and Shamey.[15] Their method models three-dimensional motion (i.e., precession and nutation), and allows for both c.g. offsets and products of inertia. The three-DOF simulation includes noninstantaneous parachute deployment models and the jettisoning of the RM's aft endcap. Because the RM has no active control system, no formal guidance and control strategy was utilized. Reference 5 describes the modeling of the simulation in greater detail.

Table 1 Exoatmospheric mission uncertainties

Properties	3-σ Variance
Mass	
Weight	±2 lb
c.g. position along spin axis	±0.25 in. (2)
c.g. position off spin axis	±0.25 in. (2)
Major moment of inertia (I_{xx}, I_{yy}, I_{zz})	±1%
Cross products of inertia (I_{xy}, I_{xz}, I_{yz})	±0.15 slug-ft^2
Post-separation state vector	
Radial position	±656 ft
In-track position	±8202 ft
Cross-track position	±1312 ft
Radial velocity	±0.66 ft/s
In-track velocity	±1.08 ft/s
Cross-track velocity	±1.12 ft/s
Pitch/yaw attitude	±1.5 deg } correlated
Pitch/yaw rate	±0.3 deg/s } correlated
Roll rate	±22 deg/s
Solid-rocket event	
Burn initiation time	±0.5 s
Rocket motor temperature	±10° F
Impulse	±0.5%
Thrust vector cant angle	±0.45 deg
Yo-yo event	
Despin initiation time	±0.5 s
Terminal roll rate	±3.75 rpm
Separation	
Spring induced velocity	0.226 ft/s

Table 2 Atmospheric mission uncertainties

Uncertainties	3-σ Variance
Transitional aerodynamics	
C_A	±5%
C_N, C_Y	±0.06
C_m, C_n	±0.01
Continuum aerodynamics above Mach 10	
C_A	±2%
C_N, C_Y	±0.05
C_m, C_n	±0.003
Continuum aerodynamics below Mach 5	
C_A	±10%
C_N, C_Y	±0.05
C_m, C_n	±0.005
Dynamic stability coefficients, C_{mq}, C_{nr}	±50%
Pressure, GRAM-95 model	3-σ scale factors (3)
Density, GRAM-95 model	3-σ scale factors (3)
Winds, GRAM-95 model	3-σ scale factors (9)
Parachute deployment altitude (pilot/drogue)	±1000 ft
Parachute deployment altitude (main)	±500 ft
Parachute aerodynamics, C_A	±20%

Numerous sources of uncertainty affect the METEOR flight model. One source for this uncertainty arises through system capability limitations (e.g., the attitude control system on the SM can only achieve the prescribed pointing direction to within a specified tolerance). A lack of knowledge concerning the flight-day density, pressure, and winds and the computational uncertainty of the aerodynamics analysis are also contributing sources of error. Furthermore, measurement limitations in the mass, moments of inertia, c.g., and thrust nozzle alignment will also result in uncertainties. In this analysis, an attempt was made to conservatively quantify and model the degree of uncertainty in each mission parameter.

For this mission, 57 potential uncertainties were identified. These uncertainties are grouped into two categories (exoatmospheric and atmospheric) and are listed in Tables 1 and 2, respectively, along with the corresponding 3-σ variances. As seen, a few of the uncertainties have multiple entries (in parentheses) to account for variations at different mission phases. For example, in Table 1 there are two separate c.g. off-axis position uncertainties (denoted by a 2 in the parentheses). The first uncertainty is applied prior to the deorbit burn

to account for c.g. measurement errors before launch, whereas the second uncertainty is applied after the deorbit burn to account for unsymmetrical burning. For modeling the atmospheric properties pressure and density, three separate uncertainties are used (denoted by a 3 in the parentheses) for each parameter to provide a variation with altitude (high, mid, and low). For the atmospheric winds, three separate uncertainties are used to provide variation in wind direction (north–south, east–west, and vertical) within each altitude band (high, mid, and low), thus, a total of nine uncertainties in all (denoted by a 9 in the parentheses).

Note that most of the 3-σ variances listed in Tables 1 and 2 were not obtained through a rigorous statistical analysis. Rather, these values are estimates based on the judgment of various experts in the field. Each of these quantities were derived independently of previous program estimates. The aerodynamic and atmospheric uncertainties were based on NASA Langley Research Center estimates. However, the estimates for many of the exoatmospheric and mass-property uncertainties were obtained through deliberations with personnel from the Jet Propulsion Laboratory, The Aerospace Corporation,[4] Kaman Sciences Corporation,[16] Morton Thiokol, Ball Aerospace,[15] EER Systems, Inc.,[17] CTA Space Systems,[18] NASA Goddard Space Flight Center, and NASA Wallops Flight Facility.

Results and Discussion

Nominal Mission

Figures 3a and 3b show the groundtrack of the nominal entry trajectory, where the major mission events are highlighted. The splashdown point is at a latitude of 36.93° N and a longitude of 73.87° W, which is about 95 n mi off the coast of Virginia. Table 3 lists the nominal set of mass properties of the RM. Note (Table 3) that the

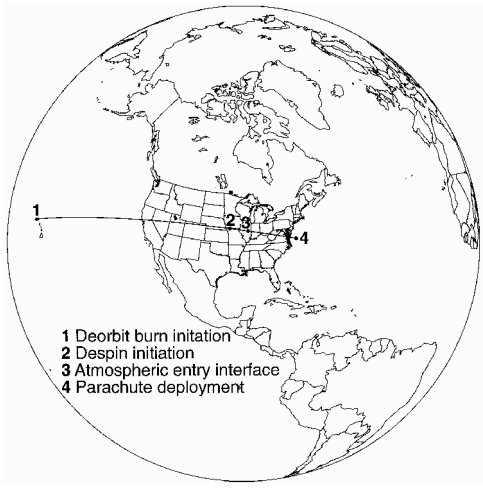

a) Global view

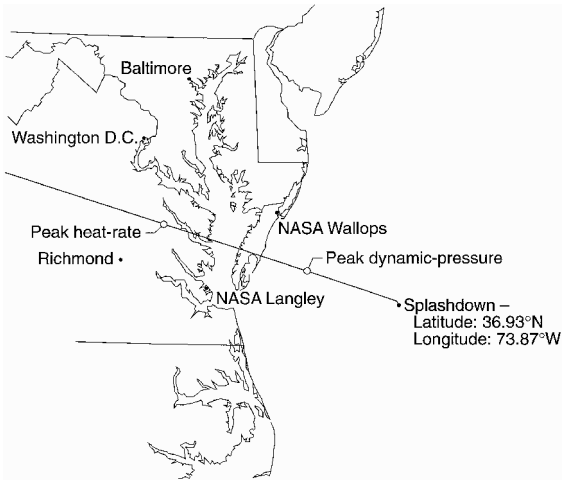

b) Terminal mission segment

Fig. 3 Nominal mission groundtrack.

Table 3 Nominal mass properties of the RM

	Deorbit	Entry
Weight, lb	763.0	686.5
Center of gravity, ft		
Along spin axis (x direction, from nose)	1.713	1.597
Off spin axis (y direction)	−0.00161	−0.00161
Off spin axis (z direction)	−0.00213	−0.00213
I_{xx}, slug-ft^2	46.40	46.23
I_{yy}, slug-ft^2	41.58	40.43
I_{zz}, slug-ft^2	40.47	39.15
I_{xy}, slug-ft^2	0.0191	0.019
I_{xz}, slug-ft^2	−0.0191	−0.0185
I_{zz}, slug ft^2	0.027	0.0261
Engine cant angle, deg	0.22	0.22

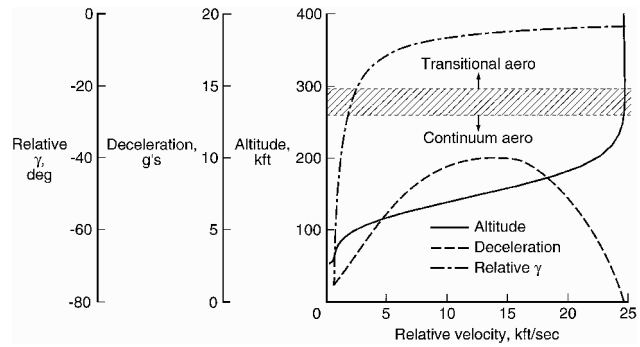

a) Entry sequence

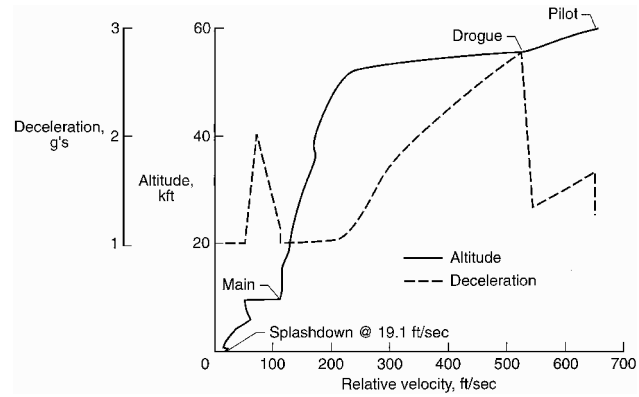

b) Parachute deployment sequence

Fig. 4 Nominal mission profile.

RM has a small nominal engine cant angle value; thus, the nominal engine thrust vector does not go through the c.g. of the vehicle (see Acknowledgments).

Figures 4 and 5 show flight characteristics of the nominal entry profile. The vehicle aerodynamically decelerates from approximately 25,000 ft/s to subsonic speed. During this time, the vehicle's aerodynamic stability reduces the total angle of attack to a moderate value (near 15 deg), as shown in Fig. 5. Peak heating occurs near Mach 21 with an angle of attack between 15 and 20 deg. The nominal attitude motion may be described by the superposition of two cycles, one in α and the other in β, each of which is centered on 0 deg. Because the two cycles are out of phase, the total angle of attack α_T (defined as the angle between the velocity vector and the vehicle's axis of symmetry) never reaches 0 deg. As seen in Figs. 4a and 5, a majority of the vehicle's attitude decrease occurs while flying in the transitional aerodynamic regime. This occurrence is the reason for the computational investment in the DSMC flowfield solutions. Without these computational solutions, the validity of this diminishing attitude motion (which is critical to mission success) would be questionable.

Also shown in Fig. 5 is an increase in the total angle of attack toward the end of the entry. This behavior is an outcome of the sharp decrease in flight-path angle observed at the end of the entry

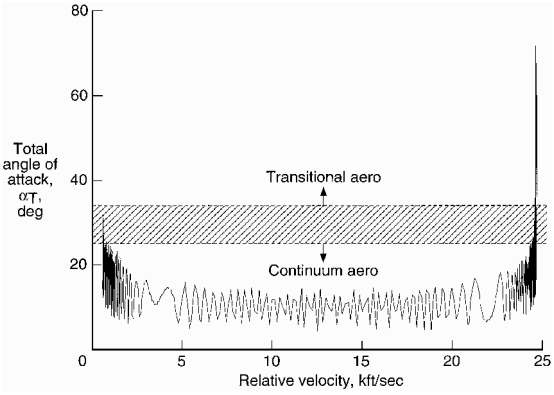

Fig. 5 Nominal mission attitude profile.

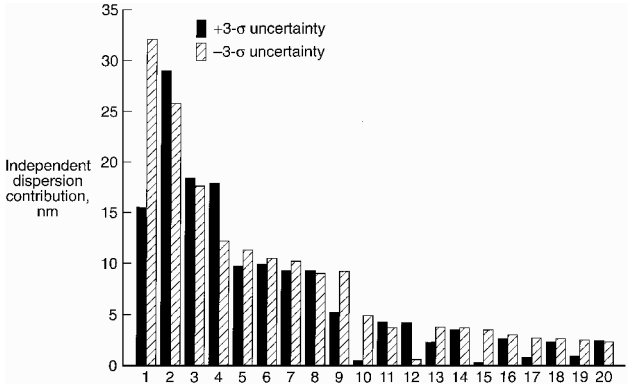

Fig. 6 Significant contributors to the total splashdown range dispersion.

(Fig. 4a). This area is also the region of flight (lower velocities) in which dynamic-stability issues begin to dominate. If the vehicle was dynamically unstable, the RM would not be able to follow this flight-path angle drop and extremely high angles of attack would result. In the extreme case, a tumbling motion could result prior to parachute deployment. However, because the vehicle is dynamically stable at all but the smallest total angles of attack, a tumbling motion does not occur. Rather, the vehicle's dynamic stability helps to minimize the effect of the flight-path angle variations. Consequently, the total angle of attack at parachute deployment for the nominal mission is on the order of 25 deg.

Beginning at an altitude of 60 kft (approximately Mach 0.8), a series of three parachutes are deployed, which slow the RM down to approximately 19 ft/s prior to splashdown. Each of these parachute deployments is evident in Fig. 4b.

Independent Uncertainty Effects

To identify the mission uncertainties that have the greatest impact on the splashdown dispersion, each mission uncertainty was varied independently at its respective $\pm 3\text{-}\sigma$ value. Figure 6 shows the resulting splashdown range dispersions for the largest contributors to the splashdown dispersion size. Mission uncertainties not depicted in Fig. 6 had splashdown dispersions less than 2 n mi.

As can be seen from Fig. 6, the mission parameters have a varying effect on the splashdown range dispersion. The range dispersions can be grouped into three categories: major (mission uncertainties 1 and 2), moderate (mission uncertainties 3–9), and small (mission uncertainties 10–20). The first group responsible for the largest range dispersions, on the order of 25–30 n mi, only include the exoatmospheric uncertainties. These uncertainties produce the largest dispersion because they alter the deorbit burn direction. For example, a c.g. offset (mission uncertainty 1) causes a change in the location of where the thrust vector is applied from the nominal mission, producing the large splashdown range dispersion. The second group of uncertainties produce range dispersion on the order of 10–20 n mi. Included in this group are several exoatmospheric effects (specific impulse, rocket-nozzle cant angle, and the initial

Table 4 Major contributors to total splashdown range dispersion[a]

Uncertainty		Dispersion with $+3\text{-}\sigma$ uncertainty, n mi	Dispersion with $-3\text{-}\sigma$ uncertainty, n mi
1	Deorbit off-axis c.g. (0.25 in.)	15.5	32.1
2	Initial attitudes/rates	29.0	25.8
3	I_{sp} (0.5%)	18.4	17.6
4	Rocket nozzle cant angle (0.45 deg)	17.9	12.2
5	Initial weight (2 lb)	9.7	11.3
6	Mid-altitude density (GRAM 95)	9.9	10.5
7	Low-altitude, east wind (GRAM 95)	9.3	10.2
8	Low-altitude, north wind (GRAM 95)	9.3	9.0
9	Entry off-axis c.g. (0.25 in.)	5.2	9.2
10	Deorbit burn initiation (0.5 s)	0.5	4.9
11	I_{xz} (0.15 slug-ft^2)	4.3	3.7
12	Solid-motor temperature (10° F)	4.2	0.6
13	Atmospheric roll rate (5%)	2.3	3.8
14	Cross-track velocity error (1.12 ft/s)	3.5	3.7
15	Radial velocity error (0.66 ft/s)	0.3	3.5
16	Cross-track position error (1312 ft)	2.6	3.0
17	I_{xy} (0.15 slug-ft^2)	0.8	2.7
18	Radial position error (656 ft)	2.3	2.6
19	I_{xx} (1%)	0.9	2.5
20	I_{yy} (1%)	2.4	2.3
Approximate $3\text{-}\sigma$ total		53.6	61.0

[a] $3\text{-}\sigma$ variance shown in parentheses.

weight uncertainties) and several atmospheric effects (mid-altitude density and low-altitude horizontal and vertical wind uncertainties). The third group of uncertainties produce range dispersions less than 5 n mi. These uncertainties include those resulting from initial state-vector errors, moments of inertia misprediction, variation in the atmospheric roll rate, and propulsion system unknowns (temperature and burn initiation time).

As seen in Fig. 6, some of the mission uncertainties have a drastic difference in the range dispersion between the $+3\text{-}\sigma$ and $-3\text{-}\sigma$ values (mission uncertainties 1, 9, 10, 12, 15, 17, and 19). This outcome is due to the RM having a nonzero nominal engine cant angle value. Consequently, when the $\pm 3\text{-}\sigma$ values are applied (for one of these mission uncertainties), one bound heightens the effect of the engine cant angle, and the other boundary value counteracts this effect. If there was no nominal engine cant angle, the resulting range dispersions caused by the $\pm 3\text{-}\sigma$ uncertainties would be more symmetric.

The one-variable-at-a-time results are summarized in Table 4. Note that relative to the exoatmospheric unknowns, the atmospheric uncertainties do not have a major impact on the splashdown range dispersion. Furthermore, the aerodynamic uncertainty associated with the mission has a minimal impact on the splashdown dispersion size. Computing the L_2 norm of these one variable at a time results, an upper bound on the resulting $3\text{-}\sigma$ range dispersion from the Monte Carlo analysis of no more than 50–60 n mi is expected.

Multiple Uncertainty Effects

To determine the effects of multiple uncertainties occurring during the entry, a Monte Carlo analysis is performed. Over 3500 random trajectories were simulated to assure a Gaussian distribution of the 57 mission uncertainties.

For some Monte Carlo cases, a high-amplitude oscillatory behavior in the total angle of attack near the atmospheric interface was observed. As a result, for this vehicle, the total angle of attack at the atmospheric interface is difficult to pinpoint. This behavior can be observed in Fig. 7 (starting at an altitude of 500 kft) for a particular Monte Carlo case where the total angle of attack at the atmospheric interface can be anywhere between 60 and 120 deg. This phenomenon is a consequence of high pitch and yaw energies, which are produced during the deorbit burn due to the thrust vector misalignment, cant angle, and the c.g. uncertainty. During the early stages of the mission, these pitch and yaw energies are suppressed by the high roll rate (73 rpm) of the vehicle, which provides inertial stability. With the RM despun to 6 rpm prior to atmospheric entry, roll stability is reduced and the pitch and yaw rates dominate

Table 5 Summary of Monte Carlo analysis

	Mean	Minimum	Maximum	3-σ
Attitude dispersion				
Mean atmospheric interface α_T, deg	66.8	36.6	111.4	26.2
Amplitude about mean atmospheric interface α_T, deg	17.2	1.6	65.2	28.7
Peak heating α_T, deg	20.6	8.5	56.7	12.8
Parachute deployment α_T, deg	51.4	14.9	170.5	56.7
Splashdown dispersion				
Splashdown downrange, n mi	2.6	−43.8	67.0	43.3 (long) −33.5 (short)
Splashdown crossrange, n mi	−0.5	−11.5	10.9	10.0
Total splashdown range, n mi	11.0	0.2	67.6	23.8
Splashdown latitude, deg	36.83	36.52	37.17	0.26
Splashdown longitude, deg	286.10	285.22	287.40	0.76

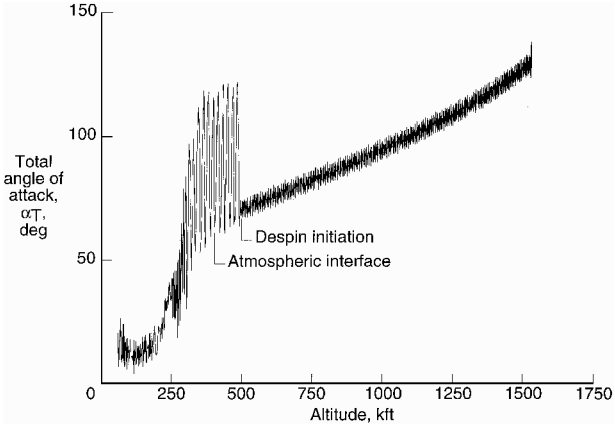

Fig. 7 Oscillatory motion in total angle of attack.

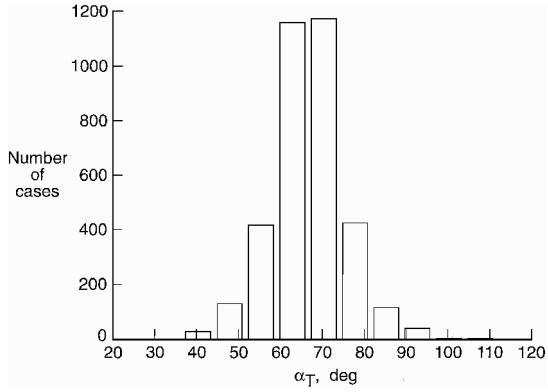

Fig. 8 Distribution of the mean total angle of attack at the atmospheric interface resulting from over 3500 Monte Carlo simulation cases.

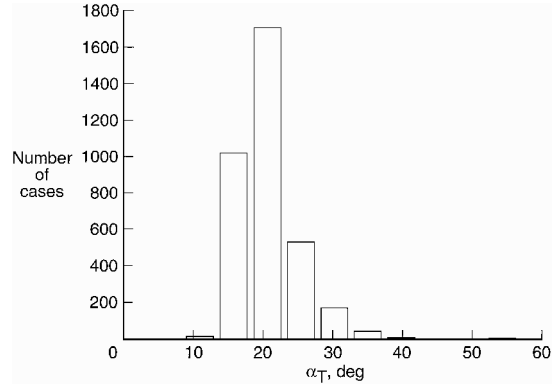

Fig. 9 Distribution of total angle of attack at peak heating resulting from over 3500 Monte Carlo simulation cases.

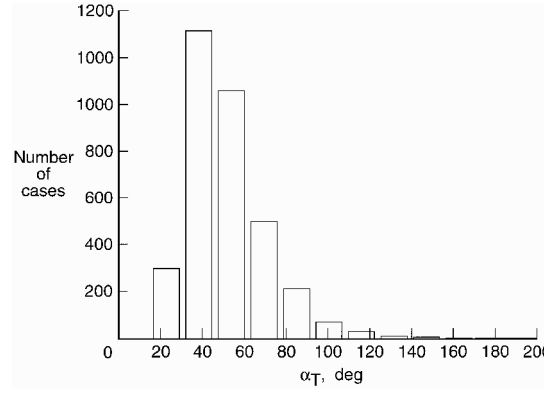

Fig. 10 Distribution of total angle of attack at parachute deployment resulting from over 3500 Monte Carlo simulation cases.

the rotational motion. This behavior is not present in the nominal mission (Fig. 5). However, a slight perturbation in one or a combination of the mission uncertainties can lead to this oscillatory motion. Approximately 25% of the Monte Carlo cases displayed this behavior.

As a result of the oscillatory motion, the mean value of this oscillatory motion in the total angle of attack at the atmospheric interface is used to express the true attitude of the RM. Figures 8–10 show the distribution of the total angle of attack at atmospheric interface, peak heating, and parachute deployment for the 3500 Monte Carlo cases. At the atmospheric interface, the statistical mean of the mean total angle of attack of these 3500 Monte Carlo cases is 66.8 deg with an oscillation amplitude of 17.2 deg. At peak heating and parachute deployment, the mean total angle of attack of the 3500 Monte Carlo cases is 20.6 and 51.2 deg, respectively. The maximum total angle of attack at each of these events can be significantly higher than these statistical mean values. Maximum values of 176.6 deg (111.4 deg plus a 65.2-deg oscillation) at atmospheric interface, 56.7 deg at peak heating, and 170.5 deg at parachute deployment were obtained. Table 5 summarizes these statistical results for the 3500 Monte Carlo cases. Note that the heatshield design limit on the total angle of attack at atmospheric interface of 75 deg is violated in some cases. However, because the frequency of the oscillatory motion is high, the heating levels on the side and aft end of the RM (for these high total angle-of-attack cases) were determined to be acceptable (see Acknowledgments). In addition, the reliability of the aerodynamic database for high altitudes and angles of attack greater than 145 deg is questionable, because these conditions exceed the limit of the database. Approximately, 0.3% of the Monte Carlo cases had total angles of attack greater than 145.0 deg.

Figures 11 and 12 show the downrange and crossrange distribution at splashdown of the 3500 Monte Carlo cases, respectively. The minimum downrange is −43.8 n mi (short) from the nominal splashdown point, whereas the maximum downrange is 67.0 n mi (long). The maximum crossrange obtained is 11.5 n mi from the nominal splashdown point. A 3-σ dispersion footprint with axes of 43.3 (long), −33.5 (short), and ±10.0 n mi (crossrange) can be constructed. Within the assumptions of the present analysis, a 99.73% probability exists that the RM will splashdown within this 3-σ footprint. Table 5 summarizes these and other statistical results.

Table 6 Summary of previous entry dispersion analysis

Mission uncertainty	Space Industries[a] dispersion, n mi	Aerospace Corp.[b] dispersion, n mi
One-at-a-time results		
Atmosphere (20%,[a] 10%[b])	14.0	8.5
I_{sp} (0.25%[a,b])	10.3	13.5
Ballistic coefficient (5.0 lb/ft^2[b])	N.A.	9.6
Drag coefficient (10%[a])	6.2	N.A.
Atmospheric roll rate (3.75 rpm[a])	6.3	0
Initial attitude (0.7 deg,[a] 0.5 deg[b])	6.2	0.8
Initial weight (1.2 lb[a])	6.0	0
State vector	5.9	3.2
Winds	4.2	0
Deorbit burn initiation (0.65 s,[a] 1.0 s[b])	2.4	0.2
Parachutes	2.0	0
Solid-motor temperature (5° F[a])	2.0	0
Thrust cosine loss (1.5 deg[a])	1.0	0
Monte Carlo results		
Downrange, n mi	22.4 (long) −22.4 (short)	17.0 (long) −17.0 (short)
Crossrange, n mi	3.8	2.9

[a]Reference 3. [b]Reference 4.

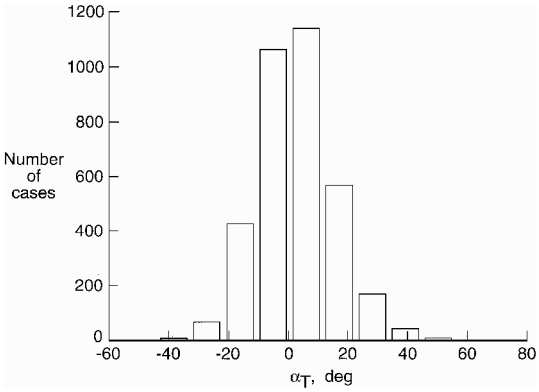

Fig. 11 Downrange distribution at splashdown resulting from over 3500 Monte Carlo simulation cases.

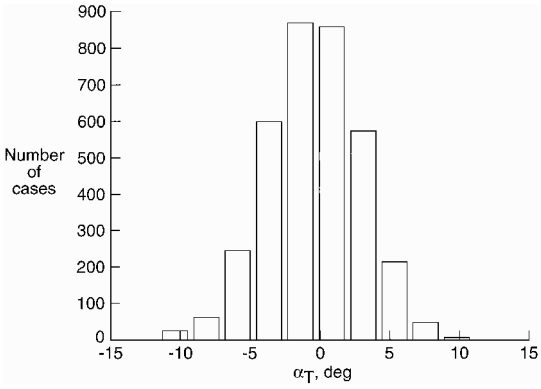

Fig. 12 Crossrange distribution at splashdown resulting from over 3500 Monte Carlo simulation cases.

Figures 13 and 14 show the atmospheric interface and splashdown locations for each of the 3500 Monte Carlo cases. Note that the total downrange dispersion shown in these figures is similar. This outcome is due to the dominant effect that the exoatmospheric uncertainties have on downrange. While impacting downrange to some extent, the atmospheric uncertainties have a more pronounced effect on crossrange. Additionally, there is a slightly higher probability (58%) that the trajectory will splashdown long than short.

The present results predict a larger splashdown range dispersion than previous METEOR entry dispersion analyses that were performed early in the program.[3,4] Table 6 summarizes the findings from Refs. 3 and 4. The splashdown predictions from the present analysis are approximately double that of Refs. 3 and 4.

Fig. 13 Range dispersion at atmospheric interface resulting from over 3500 Monte Carlo simulation cases.

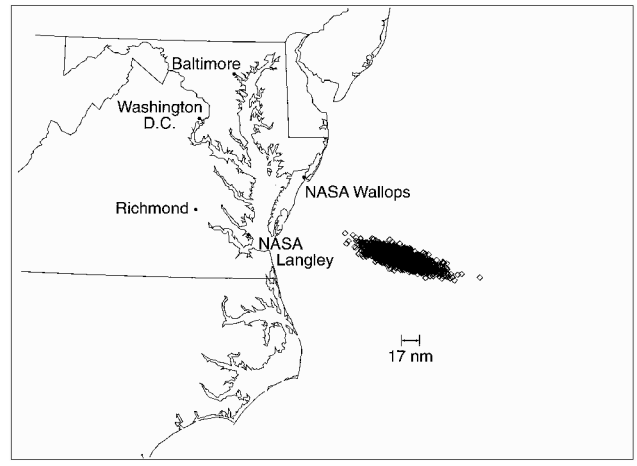

Fig. 14 Range dispersion at splashdown resulting from over 3500 Monte Carlo simulation cases.

The differences in these results can be attributed to many factors. The initial orbit altitude, target landing site, and mass properties of the RM have changed. Also, more mission uncertainties are considered in the present analysis than in the previous studies. These additional uncertainties add to the overall range dispersion. Furthermore, the 3-σ variances selected in the present study are based on more conservative estimates (roughly twice that of the previous studies in some cases, e.g., I_{sp}, solid-motor temperature, weight, and initial attitude/rates). Moreover, the aerodynamic characteristics of the RM are much better known due to the extensive computational and experimental investment. Overall, the present analysis produced a more conservative estimate of the splashdown range dispersion.

Summary

In the present study, a six-DOF entry dispersion analysis for the METEOR RM is performed. For this mission, 57 potential exoatmospheric and atmospheric uncertainties were identified. From a one-variable-at-a-time uncertainty analysis, where each variable was set at its estimated $\pm$3-σ uncertainty value, a c.g. offset from the spin axis and initial attitude/rate uncertainties where shown to produce the greatest dispersions (each on the order of 30 n mi). Uncertainties in specific impulse, engine cant angle, initial weight, midaltitude density, and low-altitude winds produced dispersions on the order of 10–20 n mi each. All other uncertainties produced dispersions less than 5 n mi. From a Monte Carlo analysis of over 3500 random, off-nominal trajectories, a 3-σ splashdown dispersion footprint with axes of 43.3 (long), −33.5 (short), and $\pm$10.0 (crossrange) n mi was obtained. Within the assumptions of the present analysis, a 99.73% probability exists that the RM will splashdown within this 3-σ footprint. Additionally, there is a 58% probability that the RM will overshoot the nominal splashdown site. Furthermore, the

present analysis predicts a larger splashdown range dispersion than previous METEOR entry dispersion analyses.

Acknowledgments

The authors would like to extend their appreciation to numerous personnel from the Jet Propulsion Laboratory, The Aerospace Corporation, Kaman Sciences Corporation, Morton Thiokol, Ball Aerospace, EER Systems, Inc., CTA Space Systems, NASA Goddard Space Flight Center, NASA Wallops Flight Facility, and NASA Langley Research Center for their help in determining the exoatmospheric and atmospheric 3-σ mission uncertainty values used in this analysis. In particular, acknowledgment is made to M. Daniels, METEOR Mission Manager, EER Systems, Inc., for a private communication on the nominal engine thrust vector; and J. Zimmer, Aerotherm Corporation, Mountain View, California, and J. Hengle, Vice-President of Space Systems Group, EER Systems, Inc., for private communications on acceptable heating levels at high angles of attack, all in October 1995.

References

[1]Hill, S. M., "Preliminary COMET Recovery Targeting and Dispersions," AIAA Paper 92-4659, Aug. 1992.

[2]Hill, S. M., and McCusker, T. J., "COMET Recovery System Flight Dynamics," AIAA Paper 93-3693, Aug. 1993.

[3]McCusker, T. J., and Hill, S. M., "Landing Dispersions for the Commercial Experiment Transporter Recovery System," AIAA Paper 93-3695, Aug. 1993.

[4]Summerset, T. K., McLain, M. G., and Sorge, M. E., "Comet Deorbit and Reentry Error Analysis," The Aerospace Corp., Contract F04701-88-C-0089, El Segundo, CA, Aug. 1992.

[5]Braun, R. D., et al., "Six-Degree-of-Freedom Aerodynamic Assessment and Monte-Carlo Dispersion Analysis for Reentry of the METEOR Capsule," NASA TM (proposed).

[6]Rault, D. F., "Aerodynamics of the Shuttle Orbiter at High Altitudes," *Journal of Spacecraft and Rockets*, Vol. 31, No. 6, 1994, pp. 944–952.

[7]Gnoffo, P. A., "Upwind-Biased, Point-Implicit, Relaxation Strategies for Viscous Hypersonic Flows," AIAA Paper 89-1972, June 1989.

[8]Bonner, E., Clever, W., and Dunn, K., "Aerodynamic Preliminary Analysis System II. Part I—Theory," NASA-CR 182076, April 1991.

[9]Wood, W. A., Gnoffo, P. A., and Rault, D. F., "Aerothermodynamic Analysis of Commercial Experiment Transporter (COMET) Reentry Capsule," AIAA Paper 96-0316, Jan. 1996.

[10]Bowman, J. S., "Dynamic Model Tests at Low Supersonic Speeds of Project Mercury Capsule Configurations With and Without Drogue Parachutes," NASA TM X-459, Feb. 1961.

[11]Brauer, G. L., Cornick, D. E., and Stevenson, R., "Capabilities and Applications of the Program to Optimize Simulated Trajectories (POST)," NASA CR-2770, Feb. 1977.

[12]Powell, R. W., and Braun, R. D., "Six-Degree-of-Freedom Guidance and Control Analysis of Mars Aerocapture," *Journal of Guidance, Control, and Dynamics*, Vol. 16, No. 6, 1993, pp. 1038–1044.

[13]Braun, R. D., Powell, R. W., Engelund, W. C., Gnoffo, P. A., Weilmuenster, K. J., and Mitcheltree, R. A., "Six-Degree-of-Freedom Atmospheric Entry Analysis for the Mars Pathfinder Mission," AIAA Paper 95-0456, Jan. 1995.

[14]Johnson, D. L., Jeffries, W. R., Yung, S., and Justus, C. G., "Improved Global Reference Atmospheric Model (GRAM) Data Base," AIAA Paper 95-0545, Jan. 1995.

[15]Etter, J. R., and Shamey, L. J., "Kane's Dynamical Equations and an Initial Value Problem for a Spacecraft Yo-Yo Despin System," AIAA Paper 91-2746, Aug. 1991.

[16]Fudge, M. L., "COMET Position Determination Support," Kaman Sciences Corp., Contract DTOS59-91-D-00263, Alexandria, VA, April 1994.

[17]Wroblewski, S. J., and Detwiler, D., "COMPATS Recovery Module Spin Balance and Alignment," EER Systems Incorp., Vienna, VA, May 1995.

[18]Anon., "COMPATS Attitude Control System (ACS) Simulation Results," CTA Space Systems, McLean, VA, May 1995.

F. H. Lutze Jr.
Associate Editor